REPORT DOCUMENTATION PAGE

Form Approved
OMB NO. 0704-0188

1. AGENCY USE ONLY *(Leave blank)*	2. REPORT DATE	3. REPORT TYPE AND DATES COVERED
	30 Apr. 97	Final (22 Dec 95 - 21 Dec 96)

4. TITLE AND SUBTITLE

Man Portable TPV Generator System

5. FUNDING NUMBERS

DAAH04-96-C-0007

6. AUTHOR(S)

K. C. Chen and Mark K. Goldstein

7. PERFORMING ORGANIZATION NAMES(S) AND ADDRESS(ES)

Quantum Group Inc.
11211 Sorrento Valley Road
San Diego, CA 92121

8. PERFORMING ORGANIZATION REPORT NUMBER

9. SPONSORING / MONITORING AGENCY NAME(S) AND ADDRESS(ES)

U.S. Army Research Office
P.O. Box 12211
Research Triangle Park, NC 27709-2211

10. SPONSORING / MONITORING AGENCY REPORT NUMBER

ARO 35077.1-RT-ST

11. SUPPLEMENTARY NOTES

The views, opinions and/or findings contained in this report are those of the author(s) and should not be construed as an official Department of the Army position, policy or decision, unless so designated by other documentation.

12a. DISTRIBUTION / AVAILABILITY STATEMENT

Approved for public release; distribution unlimited.

12 b. DISTRIBUTION CODE

13. ABSTRACT *(Maximum 200 words)*

An 112 Watts electrical output thermophotovoltaic generator was fabricated. The generator consists of a propane supply, an atmospheric combustion burner, an ytterbia emitter mantle, a fused silica absorption filter and twelve silicon concentrator arrays cooled by circulating water. The fuel to electric power conversion is 1-2%. To provide extra power needed for cooling, a pre-mix combustion design capable of generating 140-180 Watts of power was made.

The condition for photovoltaic cooling was evaluated by measuring heat flux. The maximum heat rejection was 2.8 W/cm^2 for atmospheric combustion design, and 5.5 W/cm^2 for pre-mix combustion design. The heat transfer of several PV-heat sink assemblies under different air flow velocities and ambient air temperatures was calculated. The result showed that it is feasible to use a forced-air multi-channel heat sink to cool PV cell, provided that the generator has sufficient air flow velocity, blower power and operates at no higher than 40 °C ambient air temperature.

To improve the generator portability, shock absorbers were used to lessen impact force on the emitter mantle and demonstrated a six-folds increase in vertical drop distance. Filament winding process was explored for making robust emitter structures. Self-supporting emitter structures were successfully fabricated.

14. SUBJECT TERMS	15. NUMBER IF PAGES
Superemitter, photovoltaic, dichroic mirror, generator thermophotovoltaic, rare earth oxide, sol-gel, fiber	37
	16. PRICE CODE

17. SECURITY CLASSIFICATION OR REPORT	18. SECURITY CLASSIFICATION OF THIS PAGE	19. SECURITY CLASSIFICATION OF ABSTRACT	20. LIMITATION OF ABSTRACT
UNCLASSIFIED	UNCLASSIFIED	UNCLASSIFIED	UL

MAN PORTABLE TPV GENERATOR SYSTEM

FINAL REPORT

MARK GOLDSTEIN, Ph.D., PRINCIPAL INVESTIGATOR
K. C. CHEN, Ph.D., PROJECT MANAGER

APRIL 30, 1997

U.S. ARMY RESEARCH OFFICE

CONTRACT No. DAAH04-96-C-0007

QUANTUM GROUP, INC.
11211 SORRENTO VALLEY ROAD
SAN DIEGO, CA 92121

APPROVED FOR PUBLIC RELEASE;
DISTRIBUTION UNLIMITED.

Rights in technical data developed under the terms of this contract shall remain with Quantum Group, Inc., except that the government shall have the limited right to use such data for government purposes and shall not release such data outside the government without permission of Quantum Group, Inc. for a period of four years from the completion of the contract from which the data was generated unless the data has already been released to the general public. However, effective at the conclusion of the four-year period, the government shall retain a royalty-free license for government use of any technical data delivered under this contract whether patented or not.

The proprietary information in this report are marked by "*Quantum Group, Inc. Proprietary Information.*" This information on lines specifically identified by asterisk (*) shall not be disclosed outside the government and shall not be duplicated. The government shall have the right to duplicate, use or disclose the data to the extent provided in the funding agreement. This restriction does not limit the government's right to use information contained in the data if it is obtained from another source without restriction.

FORWORD

The technical results reported herein was accomplished under US Army STTR contract DAAH04-96-C-0007, sponsored by Department of the Army and administrated by US Army Research Office, P.O. Box 12211, Research Triangle Park, NC 27709-2211. Ms. Amy W. Wendlegass is the contracting officer and Dr. Jack Kruger is the program manager. The technical work was performed by TPV/Combustion Department personnel at Quantum Group Inc., San Diego and Optical Science Center at University of Arizona, Tucson.

Personnel directly contributing to this report were:

Quantum Group, Inc. San Diego, California

Dr. Mark Goldstein	Principal investigator
Dr. K. C. Chen	Project manager (August 1996-January 1997) Ceramic processing engineer; Emitter fabrication
Mr. David Armbuster	Project manager (January-July 1996); Mechanical engineer; System design
Mr. Steve Skinner, P.E.	Combustion engineer; Flux measurement for PV heat rejection; PV forced-air cooling calculation
Mr. Jeff Hickey	Optical engineer; Optical measurement
Mr. Pedro Samiento	Pre-mix combustion burner design and fabrication
Mr. Igor Privorotskiy	TPV generator performance testing; Flux measurement; Recuperator design
Mr. Ahn Nguyen	Mechanical engineer; Shock isolation design, fabrication and testing

Optical Sciences Center, University of Arizona, Tucson, Arizona

Dr. Jose Sasian	Program manager/Optics design
Mr. Robert Gappinger	Reflector modeling and simulation
Mr. Matthew Dubin	Interference filter and plasma filter design

TABLE OF CONTENTS

FORWORD iii

TABLE OF CONTENTS iv

LIST OF FIGURES v

LIST OF TABLES vi

A. STATEMENT OF THE PROBLEM 1

B. ACHIEVEMENTS 1

C. RESULTS FOR MULTISPECTRAL GENERATOR DESIGN 2

c.1. Multi-spectral Approach 2

c.2. Reflector, Filter and Dichroic Mirror Analyses and Testing 4

D. GENERATOR FABRICATION AND TESTING 6

d.1. Ytterbia Emitter Mantle Fabrication 6

d.2. Atmospheric Combustion Design 7

d.3. Pre-mix Combustion Design 7

d.4. Optical Simulation on Reflector Design and Testing 10

d.5. Feasibility of Forced-Air Cooling of Photovoltaic Cell 13

d.6. Recuperator Design and Testing 21

d.7. Electrical Power Output Measurement 22

E. TPV GENERATOR PORTABILITY ENHANCEMENT 24

e.1. Generator Shock Isolation and Drop Test 24

e.2. Filament-Wound Emitter Structure Development 26

e.3. Suggested Work for Phase II 28

F. REPORT OF INVENTIONS 29

G. BIBLIOGRAPHY 30

LIST OF FIGURES

Figure 1. Spectra of (a) pure ytterbia emitter; (b) pure erbia emitters; (c) mix ytterbia and erbia (50Yb/50Er) emitter. 3

Figure 2. Test setup for multi-spectral TPV generator performance evaluation. 5

Figure 3. Schematic diagram of the bench-top prototype TPV generator. 8

Figure 4. The premix combustion design. 8

Figure 5. Models used to simulate the irradiance on the PV arrays (Design 1). 11

Figure 6. The simulated irradiance distribution for (a) without reflectors; (b) with 30° top and bottom reflectors, top has 3.0 in. hole, bottom 1 in. hole 12

Figure 7. A flat bottom mirror design with annular hole has been suggested to be a another favorable compromise between slightly less irradiance uniformity and convenient airflow passage for PV cooling (Designs 2 and 3) 13

Figure 8. Axial heat flux measurements for the atmospheric and the premix combustion systems. 14

Figure 9. Heat rejection rates of configuration (iii) heat sink (B)-PV in three air flow rate 20

Figure 10. Compact recuperator was being tested for increasing the power output. 22

Figure 11. The voltage-current curve measured on a single PV array in the TPV generator 23

Figure 12. The dummy generator with the attached burnt mantle for drop test 25

Figure 13. Scanning electron micrographs of metal organic derived Yb_2O_3 emitter fiber after 1 hour heat treatment at (a) 1200° C (500x), (b) 1500° C (1000x), and (c) 1600° C (1000x) 27

Figure 14. Ytterbia emitter structures made from several filament winding techniques. 27

Figure 15. (a) A self-standing helical wound emitter structure, (b) emitter structure under preliminary testing; (c) emitter structure under higher magnification showing openings for easy gas flow; (d) no cracks were observed in polished cross-section of the emitter fiber after heat treatment at 1500 °C. 28

LIST OF TABLES

Table 1. Integrated total available energies for the ytterbia-erbia mantles. 6

Table 2. Power outputs of Yb and Er mantles measured with Si and GaSb PV cells..... 6

Table 3. The power outputs (no load) of two premix emitter-burner designs. 9

Table 4. The total fluxes and percentages of waste for different top and bottom mirrors configurations..... 11

Table 5. The PV layer configuration, and thermal resistance calculated for a 6 cm x 6 cm SunPower HEDA 300 PV array. 14

Table 6. The thermal resistances and heat rejection rates of three multi-channel heat sinks described by Kleiner. 15

Table 7. The total heat transfer and heat fluxes for three configurations of heat sink/PV cell assemblies. 16

Table 8. The calculated heat sink parameters for Wakefield Engineering convoluted heat sink Part No. 270458005 and microchannel heat sink, Design B, described by Kleiner. 17

Table 9. The thermal resistances of the heat sink-PV array assemblies Configurations (ii) and (iii) under different air flow velocities. 18

Table 10. Summary of heat sink performance under several ambient air temperatures and air flow rates. 19

Table 11. Summary of the performance of the configuration (iii) heat sink (B)/PV assembly in several ambient air temperatures and air flow rates under an uniform heat input of 108 Watts. 21

Table 12. Generator power outputs under different fuel input rates. 23

Table 13. Results of shock isolation tests. 25

A. STATEMENT OF THE PROBLEM

The goal of the Phase I program is to produce a proof-of-concept thermophotovoltaic (TPV) generator capable of producing at least 100 Watts DC electrical powder. The rare-earth oxide selective emitter TPV system was chosen due to its higher system efficiency over the blackbody-based systems.

The initial design concept used a multi-band emitter material (mix ytterbia-erbia) as the radiating source. An optical reflector and a designed dichroic mirror were proposed to split the multi-bands onto two matched-bandgap photovoltaic cells, namely, silicon and GaSb cell. The reflector and the dichroic mirror were to be fabricated and their geometry and optical performance optimized to maximize the power output. The preliminary tests, however, indicated that the optical system had higher than expected losses at the reflector and dichroic mirror. The multi-spectral generator will have inferior power output compared to the pure ytterbia system and have higher costs associated with the optical components and PV cells.

The alternative ytterbia prototype generator design was proposed to reach 100 Watts goal. It consists of an air-breathing propane gas system, an ytterbia emitter mantle and spectrally-matched high performance concentrator PV cells. Shock absorbers and filament-wound emitter structures were explored to improve generator portability.

B. ACHIEVEMENTS

The principal achievement of the Phase I contract is the successful demonstration of a thermophotovoltaic (TPV) generator that, despite its non-optimized design, consistently produces 100-112 Watts of power output with a fuel to electrical conversion of 1-2%, but without the loud noise and vibration as small internal combustion electrical generators. The 100 Watts goal was achieved with less than half the time allowed for the Phase I program.

The program success relied on advancements in the subsystems. The bench-top generator used the QGI-developed ytterbia emitter mantle. The easily replaceable and low cost ytterbia emitter mantle provides a clean 0.98 micron peak spectrum. The mantle was approximately 12.7 cm long and 3.8 cm in diameter. The photons were collected by twelve high concentrator silicon PV arrays (SunPower HEDA 300, 6 cm × 6 cm arrays) — a total of 432 cm^2 of PV cell area, that were cooled by a circulating water. The generator system included a pressure-regulated propane tank at 40 psi with flow rate at 12.5 scfh, an atmospheric combustion burner, a fused silica cylindrical absorption filter, top and bottom reflectors, and an innovative compact recuperator.

The size of the propane nozzle and inlet distance were adjusted to provide maximum power output. The shapes and angles of the top and bottom reflectors were simulated by Optical Sciences Center at University of Arizona to minimize the end loss and to enhance the radiant flux uniformity on the PV array. The reflector tilt angles were optimized at 30° and showed an 18% gain in generator power output.

To compensate the power consumption for PV cooling, a pre-mix combustion burner design was fabricated. It demonstrated 15 Watts electrical output (no load) on a single 6 cm by 6 cm PV

array. This value corresponds to a projected 146 Watts (under load, ff = 0.81) for a 12 PV arrays TPV generator.

Radiant heat flux measurements and heat transfer calculation showed the feasibility of using multi-channel heat sink to cool PV. The total heat transfer and heat fluxes of several PV-heat sink assemblies in different air flow velocities and ambient air temperatures were calculated.

Linear decelerator type shock absorbers increased the mantle survival distance six folds—from 2 inch (2.4 G) to 12 inches height (16.5 G). Filament-wound emitter structures were fabricated by winding sol-gel-derived fiber. Self-supporting structures having a helical winding pattern and transparent fibers were made.

It is expected that this preliminary design has higher losses in the system, therefore, the efficiency of the system has not been rigorously measured. The Phase I work to date has laid a solid foundation for further improvements. Improvements in the TPV generator efficiency, performance, durability, and portability are needed for its use as a portable battlefield device.

C. RESULTS FOR MULTISPECTRAL GENERATOR DESIGN

c.1. Multi-spectral Approach

Thermophotovoltaic (TPV) uses an incandescent emission source to generate photons that are collected and converted to electricity by photovoltaic cells. A variety of energy sources, including combustion of fossil fuels, radioisotopes, nuclear, solar, and chemical can be used to heat up the emitter materials. Currently, either broad-band blackbody or narrow-band selective emitters are used as incandescent emission sources. The narrow-band emitters are rare-earth oxide ceramics that produce photons with wavelengths in 0.2 to 2.4 micrometers range, matching the bandgaps of several PV cells. Thus, the spectrally-matched emitters offer increased efficiencies over blackbody TPV system [Good et. al.(1995), Nelson (1994)].

Phase I program was initially proposed to investigate a multi-spectral (mix ytterbia and erbia) emitter that produces photons at two distinct peaks (main peaks at 0.98 and 1.5 μm) [ARMY STTR proposal (1995)]. The generated photons were to collected and focused with a properly-shaped reflector, and separated into the two wavelength bands by a dichroic mirror (beam splitter). These two bands were to collected on Si and GaSb cells at either sides of the dichroic mirror.

Experiments were first conducted to characterize the performance of the mix ytterbia-erbia mantles in several combustion conditions before a complete laboratory generator was to be built on this concept. Mantles of pure ytterbia, pure erbia, and their mixtures were produced by relic process. These mantles were 1-1.5 inch in diameter and 3-4 inches long. Their surface radiances were measured with a spectroradiometer in an atmospheric combustion test stand, at the distance of 8 inches under the several fuel input rates (**Figure 1**). These measurements allowed the surface radiances of the mix ytterbia-erbia mantles compositions be directly compared. Methane gas was used for these tests. Several fuel input rates, from 0.81, 1.2, 1.62, 2.43, 3.35, and 4.32 kilowatts,

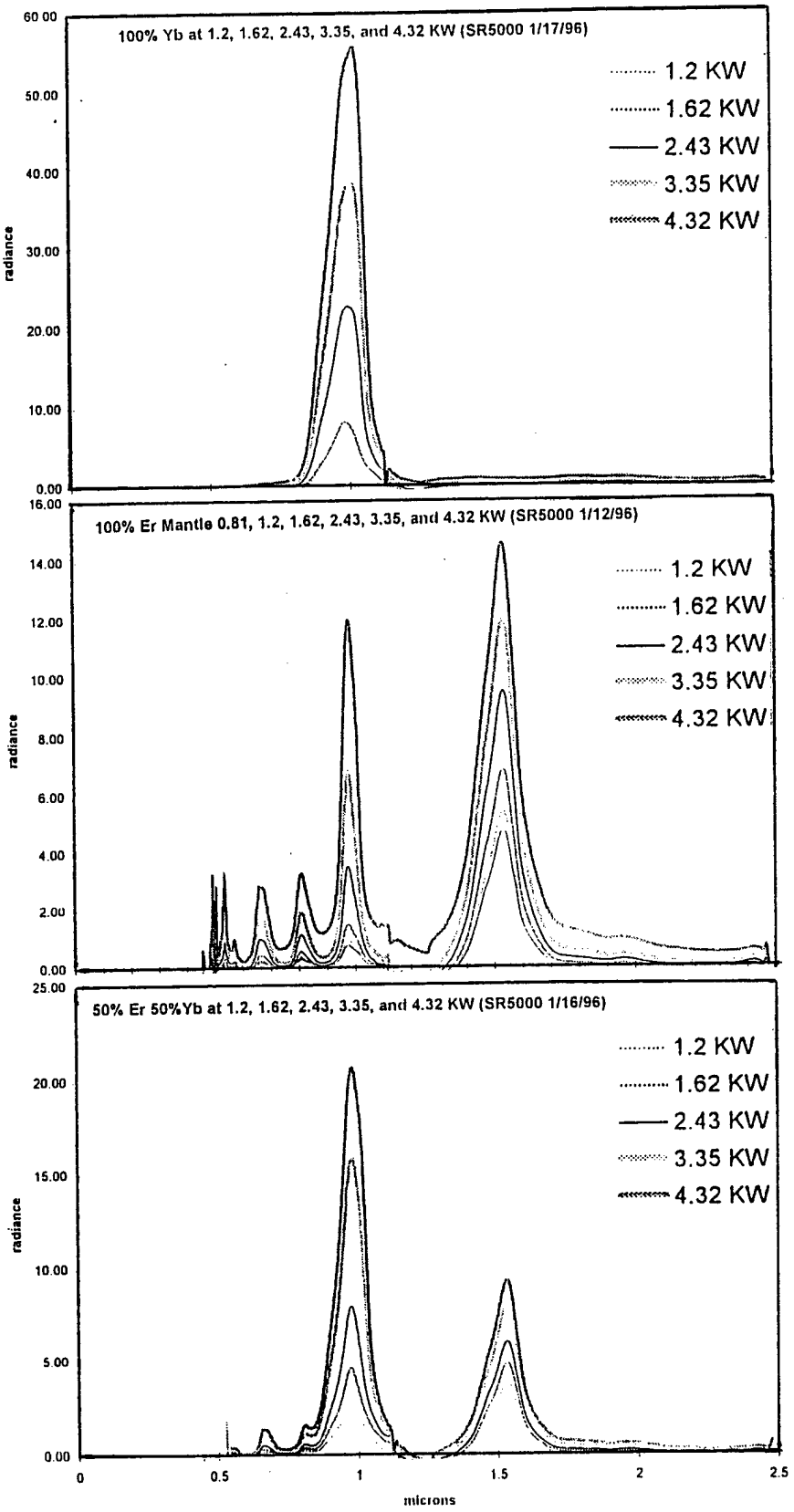

Figure 1. Spectra of (a) pure ytterbia emitter; (b) pure erbia emitters; (c) mix ytterbia and erbia (50Yb/50Er) emitter.

were used. The spectral emissions between 400 to 2500 nm were measured by focusing the spectroradiometer (SR5000 spectroradiometer, CI Systems) on the mantle surface. The spectral radiance output (in Watts/cm^2 micron) versus wavelength was calibrated with a 1200 °C blackbody cavity source, also made by CI System.

Table 1 summarizes the available energies in wattage for two PV cell bands, calculated by integrating the area under the spectra between 400 - 1100 nm (for Si cell) and 1100 - 1800 nm (for GaSb cell). The table shows that when pure ytterbia is substituted with 50% erbia, the useful ytterbia band decreases 3.1 folds (8.19/2.64), while the useful erbia band increases only 2.3 fold (1.54/0.67). Further substitution to 75% of erbia, the useful energy for the ytterbia band decrease 5.25 times (8.19/1.56), while the useful band for erbia increases only 2.52 folds (1.69/0.67). The use of the mix composition dilutes both elements in same mantle reduce their individual spectral radiant output.

The electrical power outputs were measured on ytterbia and erbia mantles with a 1 cm^2 SunPower Si cell, 0.196 cm^2 GaSb cell, and a 36 cm^2 SunPower array at every two inches between the range of 2 to 8 inches with the methane. Cooling was provided by fused silica cylinder as an absorption filter and circulating water at 7 and 20 °C. **Table 2** shows the electrical power output results measured at 2 inch distance. The electric power output measurement indicates, that the erbia emitter mantle coupled with GaSb cell generates 19% more energy over pure ytterbia with Si cell (0.176 W/cm^2 vs. 0.148 W/cm^2). However, the cost of GaSb cell is 10 times more than silicon cell. Therefore, pure ytterbia emitter with silicon PV cell has a better chance to meet the program goal within budget. The power output on a 36 cm^2 PV array is 5.4 Watts. This indicated that 100 Watts electrical output is possible by lengthening the mantle to ~6 inches (doubling the mantle surface) and using 12 PV arrays that has a total PV surface area of 432 cm^2.

c.2. Reflector, Filter and Dichroic Mirror Analyses and Testing

The University of Arizona team analyzed the reflector geometry, dichroic mirror designs, short and long pass filters for multi-spectral generator design. Various design concepts for emitter and reflector arrangement for multi-spectral generator have been reported in the February Monthly Report in details and will not be described here.

The use of either interference or absorption filters to prevent long wavelength to heat up PV cells was examined. The interference short pass filter reflects the long wavelength energy, but has a strong variation of performance with incident angle. Because the mantle emitter source is Lambertian, there are very few arrangements that can minimize the variation in incident angle. A second disadvantage of the interference filter is that a very complicated multi-layer structure is required to reflect two widely-separated long wavelength peaks. The difficulty is also ture for the long pass filter. The complexity of using the either short and long pass filters and their manufacturing are significant.

The absorption filter absorbs long wavelength of energy. It has the advantage of simplicity but it will re-radiate the energy it absorbs as it heats up. This means that the absorption filter needs to be actively cooled.

In short, a number of inefficiencies in the multi-spectral emitter and optical system limit the use for a multi-spectral TPV generator:

1. Analyses performed by the University of Arizona reveals a 30% loss in the light gathering efficiency of the reflector. This was attributed to incoherent alignment of light from the emitter and reflector which is focused onto the dichroic mirror.
2. There are losses due to light diverging from the lenses to the dichroic mirror (beam splitter). The best available dichroic mirror has an efficiency of approximately 75% in transmission and 99% in reflection, seriously compromising the spectrum of light that can be splitted between silicon and GaSb cells. Variation of incident angle of the light beam further reduces this efficiency. Since most dichroic mirrors are either design for normal incident or 45° incidence, efficient dichroic mirror is not available for Lambertian light source. These losses were calculated by the University of Arizona team and confirmed in laboratory tests with the dichroic mirror by Quantum Group Inc. **(Figure 2).**
3. Reflected photon losses from the surface of each PV cell are significant. All lost photons can not be recycled due to the beam splitter and alignment inefficiencies. In addition, some of the photons reflected from the PV cell surface or the lenses will be scattered.

In conclusion, the mix ytterbia-erbia emitter generator using a dichroic mirror and other optical components is not as efficient as the single band ytterbia emitter generator due to the lower photon output in the mix emitter and optical losses in the reflector and dichroic mirror. It has an inherited system complexity and higher cost. Efficient short and long pass filters were not available. These limitations led us to investigate the single band ytterbia and Si PV cells and an absorption filter for the TPV generator.

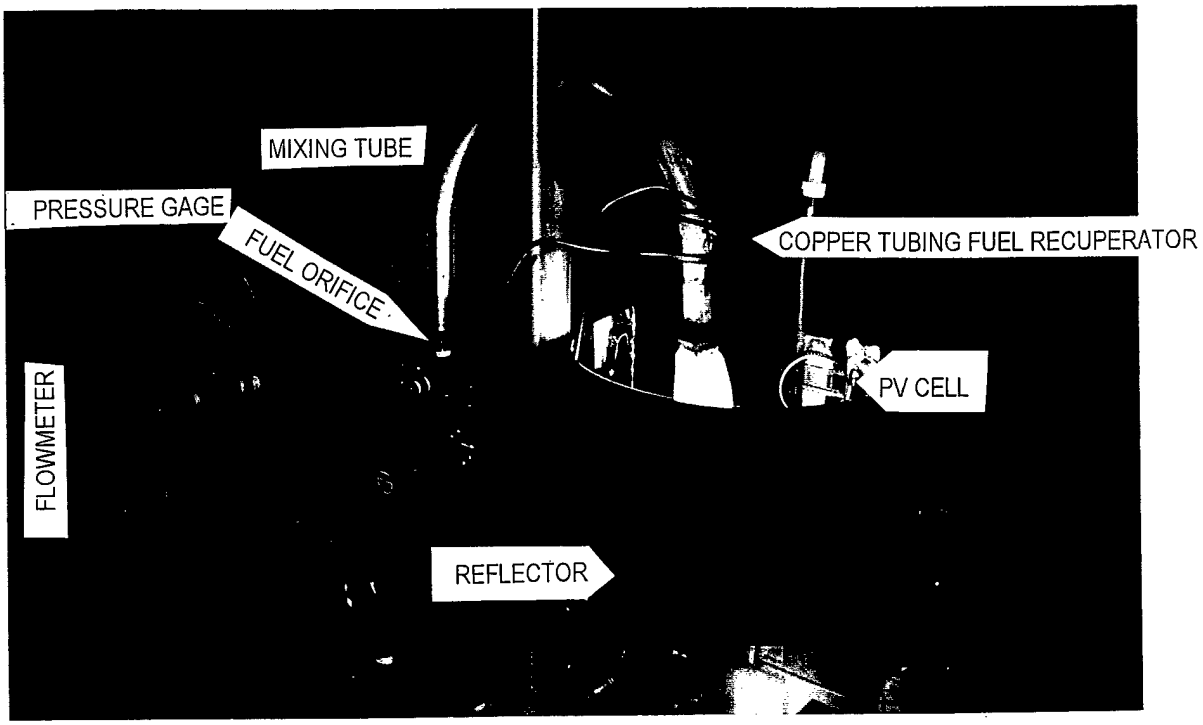

Figure 2. Test setup for multi-spectral TPV generator performance evaluation.

Table 1. Integrated total available energies for the ytterbia-erbia mantles.

Mantle Composition	Energy between 0.4 - 1.1 μm (Yb emission band) (W/cm^2)	Energy between 1.1 - 1.8 μm (Er emission band) (W/cm^2)	Total Energy between 0.4 - 1.8 μm (W/cm^2)
100% Yb	8.19	0.67	8.86
100% Er	1.49	2.83	4.32
50% Er/50% Yb	2.64	1.54	4.18
75% Er/25% Yb	1.56	1.69	3.25
25% Er/75% Yb	3.69	0.94	4.36

Table 2. Power outputs of Yb and Er mantles measured with Si and GaSb PV cells.

Emitter	PV Cell	Power Output, $Watts/cm^2$	
		With SiO_2 heat shield	Without SiO_2 heat shield
Yb	Si	0.148	0.125
Yb	GaSb	0.120	0.146
Er	GaSb	0.176	0.181

Measured at 2" distance; 3" mantle; Si cell: area = 1 cm^2, ff = 0.69;
GaSb cell: area = 0.196 cm^2; cooling water temperature = 20 °C.

D. GENERATOR FABRICATION AND TESTING

d.1. Ytterbia Emitter Mantle Fabrication:

Previous two sections conclude that pure ytterbia has the best figures of merit for 100 Watts generator design. We tested several ytterbia emitter structures, including felt, and ceramic fiber matrix burner (CFMB) developed by QGI under various programs [(ARPA (1996) and CEC (1995)] for combustion performance and power outputof the same size in similar systems. These tests indicate that ytterbia mantle structure has a superior fuel-to-photon conversion (Watts in the desired bandgap divided by Watts of fuel input) and photon flux over other ytterbia structures in the atmospheric burner system.

The ytterbia felt produced a larger amount of long IR radiation not useful to silicon PV cell. This unwanted radiation will heat up the Si cell and decreases its efficiency. This is especially pronounced with the temperature sensitive silicon cells. Additionally, a felt exhibits a large pressure drop for a combustible mixture. This high pressure drop precludes the use of felt in an atmospheric type burner, as primary air induction diminishes with increasing downstream back

pressure, ultimately affecting combustion efficiency. CFMB also exhibits a larger pressure drop than the mantle. Both felt and CFMB must incorporate a blower for combustion. The blower power requirement reduces the overall system efficiency. As a result, efforts were concentrated on an atmospheric air-breathing, mantle-based combustion system for the Phase I contract.

The ytterbia emitter mantles provided a low cost, easily replaceable structure with a clean spectrum for preliminary testing. While it is not robust, it is a consistent structure that can be used to screen generator designs. Similar to the Coleman soft mantle, before burning, it can be put into pockets for transportation without damage and it is easily replaceable after burning. Two types of emitter mantles were prepared by the relic process. The first type of mantle had an open and transparent structure, that weighted 0.013 g/cm^2 after burning. The second type of mantle had a higher knitting density and appeared to be opaque. It weighted 0.027 g/cm^2 after ignition. Power measurements indicated the dense mantle generated 40% more power than the open mantle, so that the dense mantle was used for all subsequent power output measurements.

d.2. Atmospheric Combustion Design

Figure 3 shows the air-breathing combustion system that has a Bunsen type burner with attached ytterbia mantles. The combustion gas supply was chosen to be propane, which has higher adiabatic flame temperature (2629 K) than those of methane gas (2285 K). A small (0.016 inch diameter) orifice feeded the propane into an U-shaped tube. The propane gas exited the orifice at a sufficient velocity to entrain air in the feed-tube. The gas and primary air were mixed in the U-tube, where they were preheated by the exhaust gas rising from the mantle. The distance between the orifice and tube was between 4.5 to 5.5 cm. Marked changes in power output were observed with small changes in orifice sizes and the distance from the feed tube inlet. A screen diffuser at the exit of the feed tube (entrance to the mantle) stabilized combustion.

In the early development work, an isopropanol-water filled concentric fused silica absorption filter was made, but was latter determined to be too complicated. Subsequently, a single fused silica cylinder was used as the absorption filter without cooling. Air-cooling the absorption filter will be integrated into PV cooling design in system integration in Phase II progam.

High efficiency, concentrator type Si PV arrays from SunPower, Inc., (Sunnyvale, CA, HEDA 300) were chosen for generator fabrication. New brass manifolds were designed and fabricated to assemble two 6 x 6 cm arrays vertically. This arrangement was the best compromise of size and number of PV arrays when using a 12.7 cm long mantle. The shortest distance between the mantle surface and the surface of the PV array was 3.81 cm. The system was assembled and cooling system plumbed with a NesLab water cooler operated between 7-20°C.

d.3. Pre-mix Combustion Design

* (*Quantum Group Proprietary information*) Additional power generation is needed for cooling PV
* cell, absorption filter and reflectors. A pre-mix combustion design was made to provide extra
* electric power. **Figure 4** shows the premix combustion burner, which is an integrated burner unit
* consisting a perforated cone inside ytterbia mantle, joined to an one inch diameter tee with an
* orifice, blower, and gas pressure regulators. Propane tank pressure (P_1), regulated propane

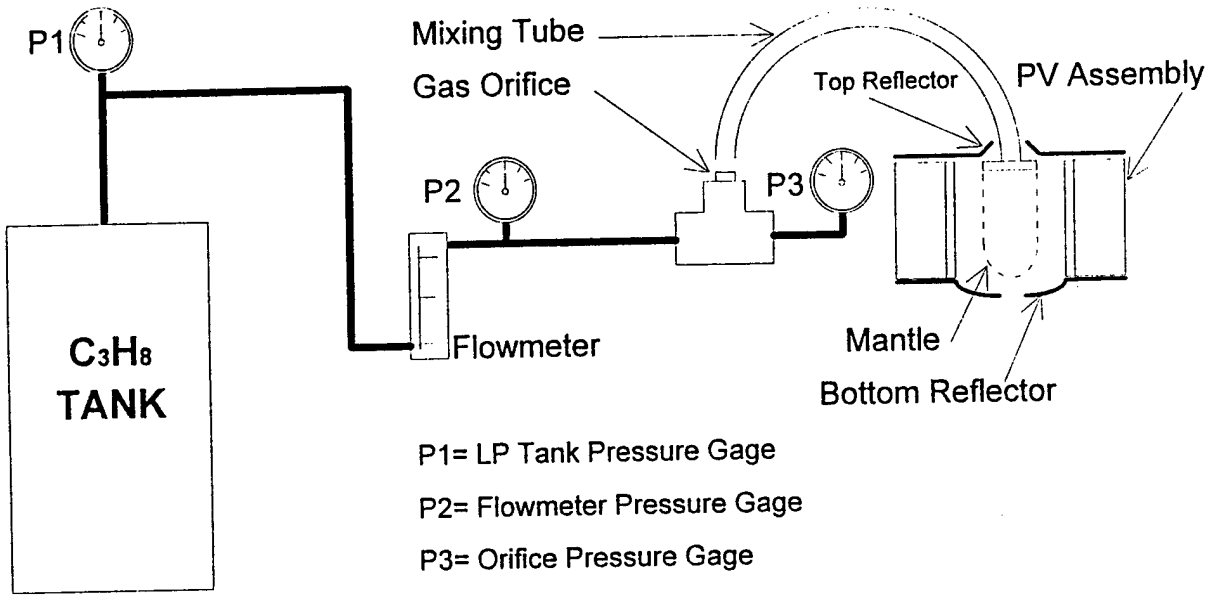

Figure 3. Schematic diagram of the bench-top prototype TPV generator.

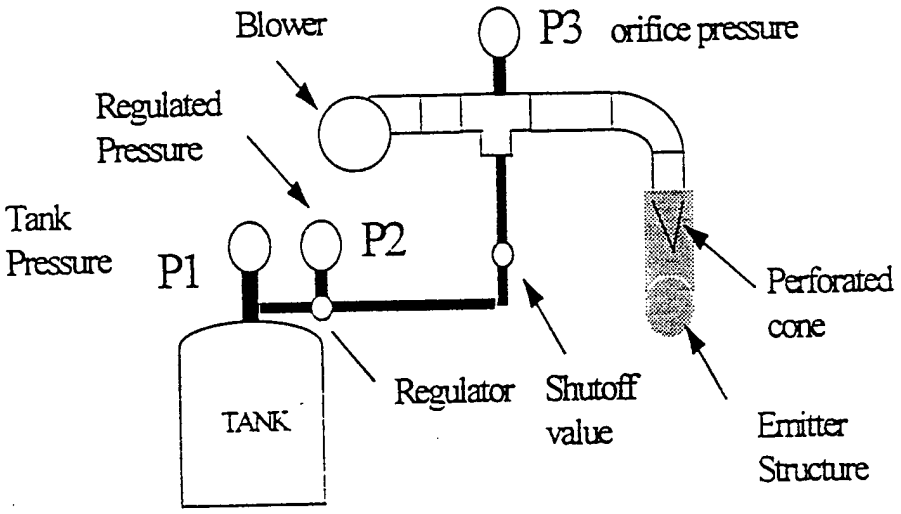

Figure 4. The premix combustion design *(*Quantum Group, Inc. Proprietary Information*).

* pressure (P_2), and orifice pressure (P_3) were simultaneously monitored. Two major variations of
* the pre-mixed designs were: hanging emitter configuration and a standing emitter design
* configuration.

The electrical power outputs were measured on a single 6 cm x 6 cm PV cell at a distance of 2.25 inch from the center of the mantle, using 20 °C circulating cooling water. Initially, the power outputs were ~11-13 Watts at a fuel input rate around 16,500-18,000 Watts. A maximum of 15 Watts of electrical power output (no load) was obtained a fuel input rate of 20,460-22,600 W (**Table 3**). This extrapolates to an no load 180 Watts of electrical power for a 12 PV arrays generator or 146 Watts under optimal loading (assuming the same uniform irradiance can be obtained on all arrays 15 Watts x 0.81 x 12 = 146 Watts). However, higher power generation also redefines the PV heat rejection and cooling requirements.

Table 3. The powers output (no load) of two premix emitter-burner designs.

Emitter-burner designs/ Fuel Input/ Cooling H_2O Temp.	P_1 psi	P_2 psi	P_3 in. H_2O	Blower VDC	Blower Amp	PV V_{oc}	PV I_{sc}	Power (unload)
Hanging Emitter Design								
Fuel input: 18,100 W								
7 °C	100	0-1	9.5	31	0.175	17.77	0.785	**14.0**
Fuel input: 20,460 W								
7 °C	110	<4	11.75			17.81	0.66	**11.8**
20 °C	100	<4	12			17.33	0.682	**11.8**
20 °C	100	0-1	12	31	0.175	17.39	0.865	**15.0**
Fuel input: 21,400 W								
7 °C	90	0-1	13	31	0.175	17.84	0.86	**15.3**
20 °C	100	0-1	13	31	0.175	17.36	0.79	**13.7**
40 °C	80	0-1	13	31	0.175	16.65	0.89	**14.8**
Fuel input: 22,600 W								
20 °C				31	0.175	17.39	0.87	15.0
Standing Emitter Design								
Fuel input: 18,000W								
7 °C	100	<4*	9	28	-	17.41	0.49	**8.5**
20 °C	98	<4*	9	28	-	16.93	0.50	**8.4**
40 °C	90	<4*	9	28	-	16.17	0.49	**7.9**
Fuel input: 20,000 W								
7 °C	105	0-1	11.5	30	-	17.69	0.619	**11.0**
20 °C	100	0-1	11.5	30	-	17.12	0.572	**9.8**
40 °C	85	0-1	11.5	30	-	16.50	0.605	**10.0**

* pressure regulator value is sensitive to adjustment.

d.4. Optical Simulation on Reflector Design and Testing

In the early part of the program, the Optical Sciences Center at University of Arizona calculated the individual optical components and light collecting performance in the TPV generator system using the Code V optical design software (Optical Research Associates). Preliminary reflector designs and end mirror simulation were obtained. Latter, a new simulation program ASAP 5.0, developed by the Breault Research Organization for the purpose of modeling vehicle headlights and tail lights, was used to analyze the TPV optical system.. The program is a fully-functional optical design software with a significant emphasis on light source-modeling basis as opposed to a pure ray tracing approach. Better simulation and more detailed illumination patterns of ytterbia mantle and more accurate results were derived by using the ASAP 5.0 software.

The simulation was to obtain maximum irradiance and uniform illumination on the PV cells by properly tilting the top and the bottom reflectors. Early simulation assumed a mantle cylinder of 2.54 cm (1 inch) diameter and 10.16 cm (4 inches) long with uniform surface radiance for simulation work. Latter, a dome-shaped end of was added to the cylinder (12.7 cm) for simulation. The geometric shapes of the reflectors, including cone, parabolic and multi-faceted, and their tilting angles were varied to obtain a maximum irradiance and uniformity on two-stacked 6 cm x 6 cm PV array **(Figure 5)**.

The modeling indicated the best irradiance uniformity can be obtained with the top and bottom mirrors both tilted at 27-30°. There was a 3 inch opening in the top mirror for hot gas to escape and an 1.0 inch opening in the bottom mirror for secondary air intake. The irradiance plots for no mirrors and the most favorable case at 30° tilt angle are shown in **Figure 6**. Alternatively, a flat bottom mirror design with annular hole was suggested to be a favorable compromise between slightly less irradiance uniformity and convenient airflow passage for PV cooling **(Figure 7)**.

The predicted power increase by adding 30° cone shape reflectors was 32.7%. However, we obtained 18% power gain by adding both top and bottom reflectors. This lower than expected power gain was attributed to the non-uniform irradiance of the emitter surface and losses due to the quartz heat filter and the reflector.

According to the simulation, no additional flux was gained by using curved reflectors. The difference in heat rejection (heat flux above the minimum plane) between the curved and the flat-shaped, and facet cone-shaped mirrors was within 0.5%. This indicates the flat mirror is better since it is cheaper to manufacture. Longer PV array than the emitter light source length did not improve the uniformity in irradiance on the PV cells. It is suggested that further improvement in the irradiance on the PV arrays can be achieved by making the PV arrays into 3 cm x 6 cm thin vertical stripes. **Table 4** summarizes the simulation results.

Table 4. The total fluxes and percentages of waste for different top and bottom mirrors configurations.

Design No.	Mirror Tilt (degree)	Top Mirror Hole Diameter (in.)	Bottom Mirror Hole Diameter (in.)	Total Flux (arbitrary unit)	Percent Waste (%)
1	25°	3.0	1.0	128130	6.6
1	30°	3.0	1.0	124510	6.7
2	no mirrors	-	-	80012	20.1
2	25°	3.0	0.5	115470	13.2
2	30°	3.0	0.5	115530	12.4
3	no mirrors	-	-	91503	19.7
3	25	3.0	0.5	131340	23.9
3	30	3.0	0.5	131140	23.4

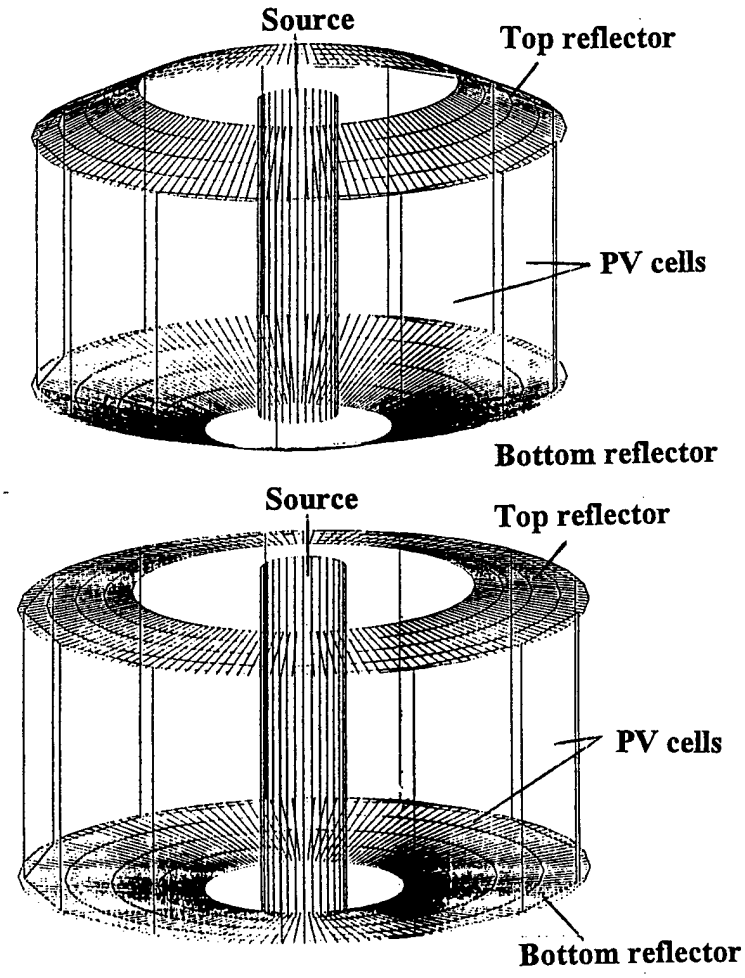

Figure 5. Models used to simulate the irradiance on the PV arrays (Design 1).

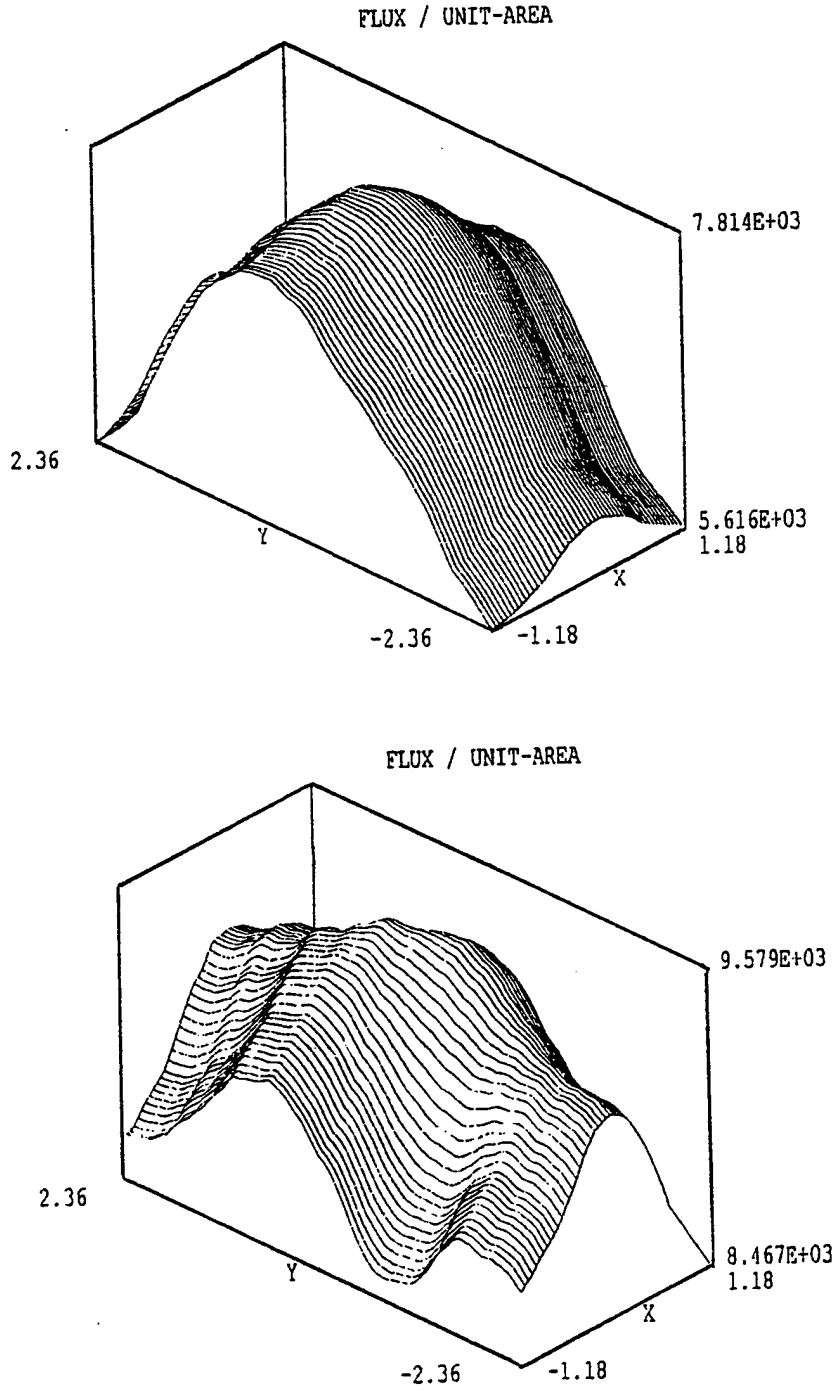

Figure 6. The simulated irradiance distribution for (a) without top and bottom reflectors; (b) with 30° top and bottom reflectors, top has 3.0 in. hole, bottom 1 in. hole

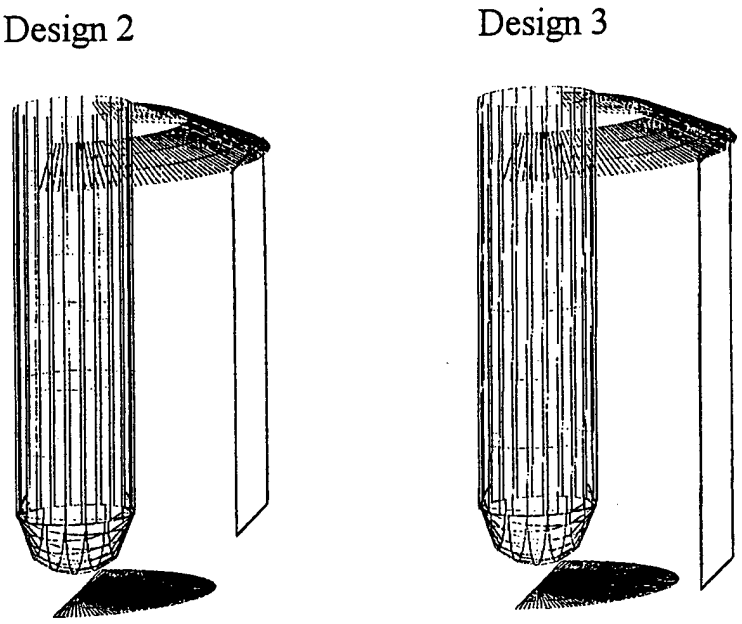

Figure 7. A flat bottom mirror design with annular hole has been suggested to be a another favorable compromise between slightly less irradiance uniformity and convenient airflow passage for PV cooling (Design 2 and Design 3 with longer PV cells)

d.5. Feasibility of Forced-Air Cooling of Photovoltaic Cell

One of the major concern of a man portable generator is the effective cooling of PV array. Since air cooling offers substantial advantage with respective to reliability, cost and ease of application over a more complex liquid cooling technique, it was evaluated in details.

Using a Gardon gauge, the heat flux profile was measured along the length of ytterbia emitter at same distance of the generator design (Medtherm Corp. Hunsville, Alabama 35804, transducer S/N 93452, H-201 meter). The results of the heat flux measurement for the atmospheric and premix designs at different fuel inputs are given in **Figure 8**. The axial heat flux measurements show the maximum heat flux for the atmospheric design is 2.8 Watts/ cm^2 and 5.5 Watts/^{cm2} for premix design. These values are used as the average heat rejection values for evaluation air-cooling capability of heat sink.

To determine the feasibility of forced-air cooling of a PV cell, we first calculated the thermal resistance of PV cell and heat sink assembly, and estimated the heat dissipation under limits set forth by the silicon PV cell (70 °C) and ambient air temperatures (25-40 °C). Based on the individual layer thickness, area, and thermal conductivity provided by the vendor (SunPower, Corporation, Sunnyvale, California), the thermal resistance of the multi-layered concentrator silicon cell (Dense Array HEDA 300) was estimated to be 0.0187 °C/W (**Table 5**).

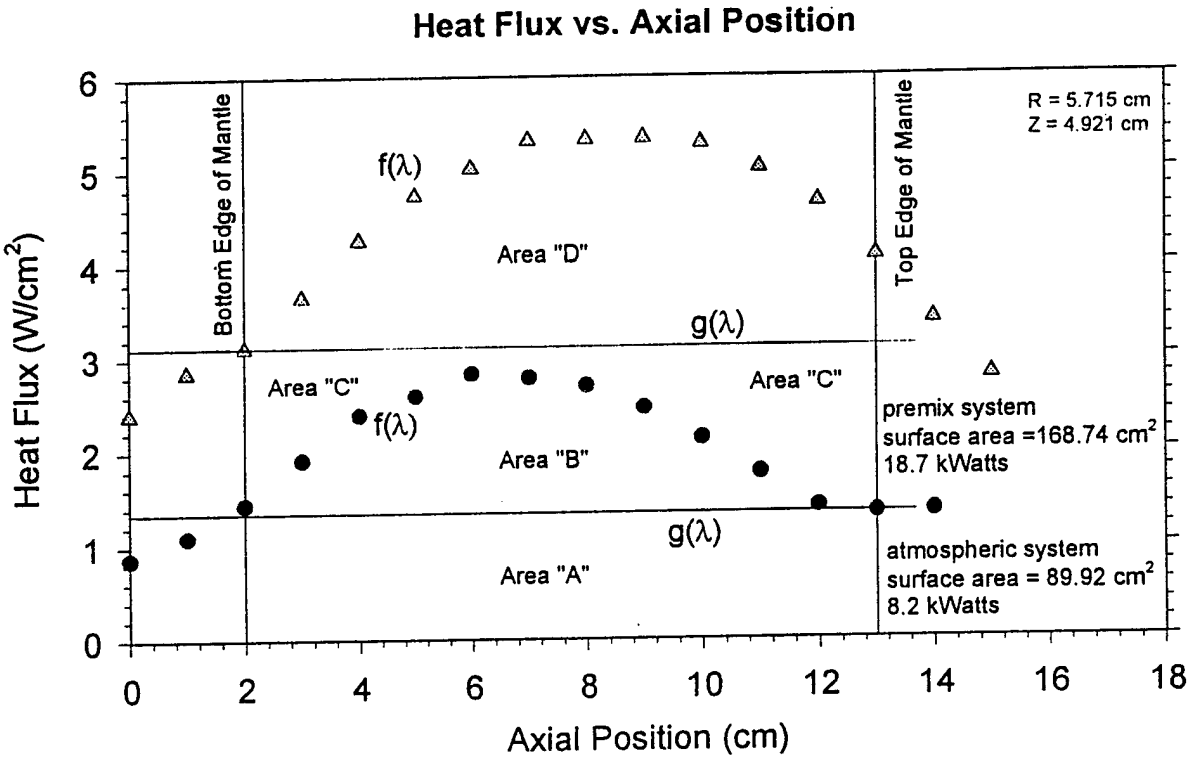

Figure 8. Axial heat flux measurements for atmospheric and premix combustion systems.

Table 5. The PV layer configuration, and thermal resistance calculated for a 6 cm x 6 cm cell from a SunPower HEDA 300 PV array.

PV cell construction	Thermal conductivity, k (W/°C·cm)	Layer Thickness L (cm)	Thermal Resistance, θ = L/kA (°C/W)	
Silicon PV cell	1.410	0.0127	0.00025	R_1
solder #1 (95% tin)	0.6211	0.0051	0.00023	R_2
Alumina (Al_2O_3)	0.2510	0.0076	0.00084	R_3
Thermal Adhesive	0.3425	0.0051	0.00041	R_4
Copper plate	3.82	0.1397	0.00102	R_5
Solder #2 (95% tin)	0.6211	0.0254	0.00114	R_6
Brass (70% Cu, 30% Zn)	1.19	0.6350	0.0148	R_7
		Total θ $=\Sigma(L_i/k_i \times A)$	0.0187	ΣR_i

(1) Reported by SunPower but was not observed under microscope
(2) PV cell area (A) = 6 cm x 6 cm

We then calculated the total heat dissipation (Q) by using the following equation:

$$Q = \Delta T/\Sigma R_i = (T_{PVcell} - T_\infty)/[(\Sigma \Delta x_i/k_i A_i) + (1/h_i A_i) + (1/h_o A_o)]$$
$$= (T_{PVcell} - T_\infty)/[(\theta_{PV} + \theta_{CS} + \theta_{SA})] \quad (1)$$

The acceptable temperature limit of PV cell (T_{PVcell}) is 70°C and the ambient air temperature (T_∞) is 40°C, assumed for a hot desert condition. Therefore, the temperature gradient ΔT is 30°C.

The total thermal resistance, ΣR_i, of the PV cell and heat sink assembly contains three terms: (1) the thermal resistance of the multi-layered PV cell ($\Sigma \Delta x_i/k_i A_i = \theta_{PV}$) as given in Table 5; (2) the thermal resistance of a thermal conductive adhesive between PV cell and heat sink, ($1/h_i A_i = \theta_{CS}$); and (3) the thermal resistance of the heat sink to the ambient air (θ_{SA}). The heat sink thermal resistance, θ_{SA} is determined by the heat sink design, geometry, orientation and air flow rate. In order to evaluate the forced-air cooling and to calculate the total heat dissipation, we need to use heat sinks with known θ_{SA} values under several air flow rates. Heat sinks capable of dissipating ~ 4 to 5 W/cm^2 at 4 W of pumping power are described by Kleiner et. al. [Kleiner (1995)]. **Table 6** tabulates the thermal resistances of three heat sinks under different air flow rate and their maximum heat rejection rates for a thermal gradient of 30°C.

Table 6. The thermal resistance and heat rejection rate of three multi-channel heat sinks described by Kleiner [Kleiner et. al. (1995)].

Heat Sink	Materials	Thermal Resistance* θ_{SA} [°C/W]	Air Flow Rate [l/s]	ΔT^{**} ($T_{PVcell} - T_\infty$) [°C]	Max. Heat Rejection Rate [W/cm^2]
A	Cu	0.238	4.67	30	5.04
B	Cu	0.249	3.87	30	4.82
C	Al	0.266	4.20	30	4.51

* 4 W pumping power, including tubes

** T_{PVcell} : PV temperature 70 °C, T_∞: ambient air 40°C

Next, we decided how to attach a heat sink to the PV array. There are few possible configurations:

(i) Direct attachment of a heat sink to the back of the current PV array using a thin layer of solder (e.g. solder #2);

(ii) Remove all other layers in the multi-layered PV and attach the heat sink directly to the silicon cells with a thermal conductive dielectric adhesive.

(iii) Modify the PV array by removing the thick brass layer (highest thermal resistance) and attach the heat sink.

Using the heat sink thermal resistance, 0.238°C/W for θ_{SA}, 0.001 °C/W for θ_{CS}, and 0.0187 °C/W for θ_{PV}, we obtained the total heat transfer Q and heat rejection rate Q" for the PV/heat sink assembly Configuration (i):

$$Q_A = \Delta T/\Sigma R_i = 30°C/(0.0187 + 0.001 + 0.238)\ °C/W = 117\ W$$

$$Q"_A = 117\ W/(6\ cm \times 6\ cm) = 3.23\ W/cm^2$$

For Configuration (ii), a heat sink is directly mounted onto the silicon cell without all other layers. This configuration requires a thin layer of dielectric and thermal conductive adhesive to isolate the PV leads and from heat sink. A 3M dielectric thermal adhesive with known thermal resistance was chosen for analysis (3M thermal adhesive 9882, thermal conductivity 0.0043 W/cm.K, 0.00508 cm thick, thermal resistance 0.0328 °C/W, 3M, Minnesota). The heat transfer and heat flux are calculated as:

$$Q_A = \Delta T/\Sigma R_i = 30°C/(0.00025 + 0.0328 + 0.238)\ °C/W = 111\ W$$

$$Q"_A = 111\ W/(6\ cm \times 6\ cm) = 3.1\ W/cm^2$$

For Configuration (iii), after removing brass resistance of 0.0148 °C/W from the PV array, the PV cell resistance is 0.0039 °C/W:

$$Q_A = \Delta T/\Sigma R_i = 30°C/(0.0039 + 0.238))\ °C/W = 124\ W$$

$$Q"_A = 124\ W/(6\ cm \times 6\ cm) = 3.4\ W/cm^2$$

Similarly, the total heat transfer and heat flux were calculated for heat sinks B and C for configurations (i)-(iii). **Table 7** summarizes the results of three heat sinks in three configurations.

Table 7. The total heat transfer and heat fluxes for three configurations of heat sink/PV cell assemblies.

	Heat Sink-PV Cell Configurations					
	(i)		(ii)		(iii)	
Heat Sinks	Q_i (W)	$Q"_i$ (W/cm^2)	Q_i (W)	$Q"_i$ (W/cm^2)	Q_i (W)	$Q"_i$ (W/cm^2)
A	117	3.2	111	3.1	124	3.4
B	112	3.1	106	3.0	119	3.3
C	105	2.9	100	2.8	111	3.1

Q: total heat transfer; Q": heat flux; i = A, B or C

These calculations show that, to a first approximation, these heat sinks are able to dissipate ~3 - 3.4 W/cm^2 — exceeding the peak heat flux of 2.8 W/cm^2 measured on the PV array in the atmospheric system.

To reduce the calculation effort and because there is a similarly-constructed multi-channel heat sink and efficiency available from Wakefield Engineering (convoluted heat sink Part No. 270458005), only the performance of the heat sink B was calculated in details (**Table 8**). Thermal resistance data of heat sink B at three different air velocities (2.5, 3.87, and 5.5 l/s) were used for detailed calculation (**Table 9**).

Table 8. The calculated heat sink parameters for Wakefield Engineering convoluted heat sink Part No. 270458005 and microchannel heat sink, Design B, described by Kleiner.

Heat Sink Parameters	Symbol[1]	Current calculation for Wakefield Engineering Heat sink Part No. 270458005	Design B reported in Kleiner et al.[1]
Heat sink width (cm)	W_{hs}	6	5
Fin length (cm)	L_{fin}	1.16	1.50
Number of fin per inch	n	27	32
Fin width (cm)	W_{fin}	0.01	0.012
Channel width (cm)	W_{ch}	0.0850	0.0506
Fin surface area (cm^2)	A_f	375	480
Heat sink total area (cm^2)	A_s	390	488
Heat sink heat transfer coefficient (W/cm·K)	h	0.0109	0.0192
Hydraulic diameter of cooling channel	D_{hch}	0.1584	0.0979
Nusselt number	$N_{u\ Dhch}$	0.8728	0.9369
Fin efficiency	η_f	0.9548	0.9731
Heat sink efficiency	η_s	0.9565	0.9735

From **Table 9,** for example, the configuration (ii) has a total thermal resistance ($\theta_{SA} + \theta_{CS} + \theta_{JC}$) of 0.384 °C/W at 2.5 liter per second of air flow velocity. Using the equation (1), with the PV cell temperature at 70 °C, the total heat transferred and heat flux at 40 °C ambient air temperatures is calculated as:

$$Q_{a1} = (70 - 40)\ °C \div (0.384\ °C/W) = 78.11\ W; \qquad Q'' = 2.2\ W/cm^2$$

Similarly, the total heat transfer and heat flux are calculated for 25, 30, 35°C ambient temperatures as well as for two other air flow velocities, 3.9 and 5.5 l/s (8.2 and 11.7 cfm). The results of these calculation are summarized in **Table 10**.

Table 9. The thermal resistances of the heat sink-PV array assemblies Configurations (ii) and (iii) in different air flow velocities.

Heat Sink Operation Conditions	PV/ heat sink configurations		
	(ii)	(iii)	
	Resistance (°C/W)	Resistance (°C/W)	
Silicon PV ◊ array configurations with dielectric thermal adhesive* or solder**	0.033*	0.0039**	$(\theta_{CS} + \theta_{JC})$
Thermal resistance of heat sink "B "			
@ Air flow rate of 2.50 l/s (5.3 cfm)	0.351		θ_{SA1}
@ Air flow rate of 3.87 l/s (8.2 cfm)	0.249		θ_{SA2}
@ Air flow rate of 5.50 l/s (11.7 cfm)	0.194		θ_{SA3}
Thermal resistance of heat sink "B" and PV cell assembly			
Case (a) Air flow rate at 2.50 l/s (5.3 cfm)	0.384	0.388	$\theta_{CS} + \theta_{JC} + \theta_{SA1}$ (case a)
Case (b) Air flow rate at 3.87 l/s (8.2 cfm)	0.282	0.253	$\theta_{CS} + \theta_{JC} + \theta_{SA2}$ (case b)
Case (c) Air flow rate at 5.50 l/s (11.7 cfm)	0.227	0.198	$\theta_{CS} + \theta_{JC} + \theta_{SA3}$ (case c)

◊ A. L. Fahrenbruch and R. H. Bube, Fundamentals of Solar Cells, Academic Press, New York 1983

* 3M Technical Data Sheets 1995, Thermally conductive adhesive transfer tapes 9882,9885,9890. 2 mils thick

From **Table 10**, we see that the heat flux, Q', values exceed 2.75 Watts/cm^2 at the air flow rates of 3.9 l/s and 5.5 l/s and 40 °C ambient air. These values are an optimistic estimation since we have to consider the air temperature rise when pass through the heat sink.

Next, the air temperature rise, $\Delta T'$, at the exit of the heat sink is calculated according to the following equation: [Wakefield Catalog (1996)]

$$\Delta T' = \frac{1.76 \times Q \times M}{V} \qquad (2)$$

where Q is the heat rejection in Watts, V is the volumetric flow rate in cubic foot per minute (cfm), $\Delta T'$ is the air temperature rise through the heat exchanger in °C, 1.76 is a constant based on 25°C air properties. For air temperatures other than 25°C, correction factors M are used (M = 1.00, 1.02, 1.04, 1.06 and 1.09 for 25, 30, 35,40 and 50 °C air, respectively). The heat transfer and heat flux for the PV cell/heat sink arere-calculated based on the average temperature at the inlet and outlet.

Table 10. Summary of heat sink performance under several ambient air temperatures and air flow rates. The last column is the heat fluxes based on the average temperatures.

PV/heat sink assembly (ii)	T_∞ (°C)	Q (W)	Q" (W/cm^2)	ΔT (T_{OUT}-T_{IN})	T_{AVE} (°C)	Q_{AVE} (W)	$Q"_{AVE}$ (W/cm^2)
Case (a) Air flow 2.5 l/s	25	118	3.3	39	45	67	1.9
	30	104	2.8	35	48	58	1.6
	35	91	2.5	31	51	50	1.4
	40	78	2.2	28	54	42	1.2
Case (b) Air flow 3.9 l/s	25	160	4.4	34	42	99	*2.8*
	30	142	3.9	31	46	87	2.4
	35	124	3.5	28	49	75	2.1
	40	106	3.0	24	52	64	1.8
Case (c) Air flow 5.5 l/s	25	198	5.5	30	40	132	*3.7*
	30	176	4.9	27	44	116	*3.2*
	35	154	4.3	24	47	101	*2.8*
	40	132	3.7	21	51	86	2.4

Italic indicates workable conditions.

As an example, for 40 °C ambient air temperature, air flow rate 2.5 l/s (5.3 ft^3/min), the air temperature at the heat sink exit is calculated as:

$$\Delta T = (1.76 \times 78.1 \times 1.06)/5.3 = 28\ °C$$

Therefore, $T_{OUT} = T_\infty + \Delta T = 40 + 28 = 68\ °C$, and

$$T_{AVE} = \tfrac{1}{2}(T_{OUT} + T_\infty) = 54\ °C$$

The average temperature T_{AVE}, is used to calculate the new total heat rejection value (Q_{AVE}) and flux ($Q"_{AVE}$) at the 70°C PV cell temperature using the equation (1):

$$Q"_{AVE} = (70 - 54)\ °C / 0.384\ °C/W = 42.3\ W$$

and $Q"_{AVE} = 1.2\ W/cm^2$

This value is less than the 2.2 W/cm^2 (row 5, column 4) calculated based on the ambient (inlet) air temperature of 40 °C. **Figure 9** summarize the calculation results.

In conclusion, this calculation shows the microchannel heat sink B can be used to dissipate up to 2.4 W/cm^2 at 70 °C cell temperature, 40 °C ambient air, slightly less than the targeted value, 2.8 Watt/cm^2 for air-breathing system.

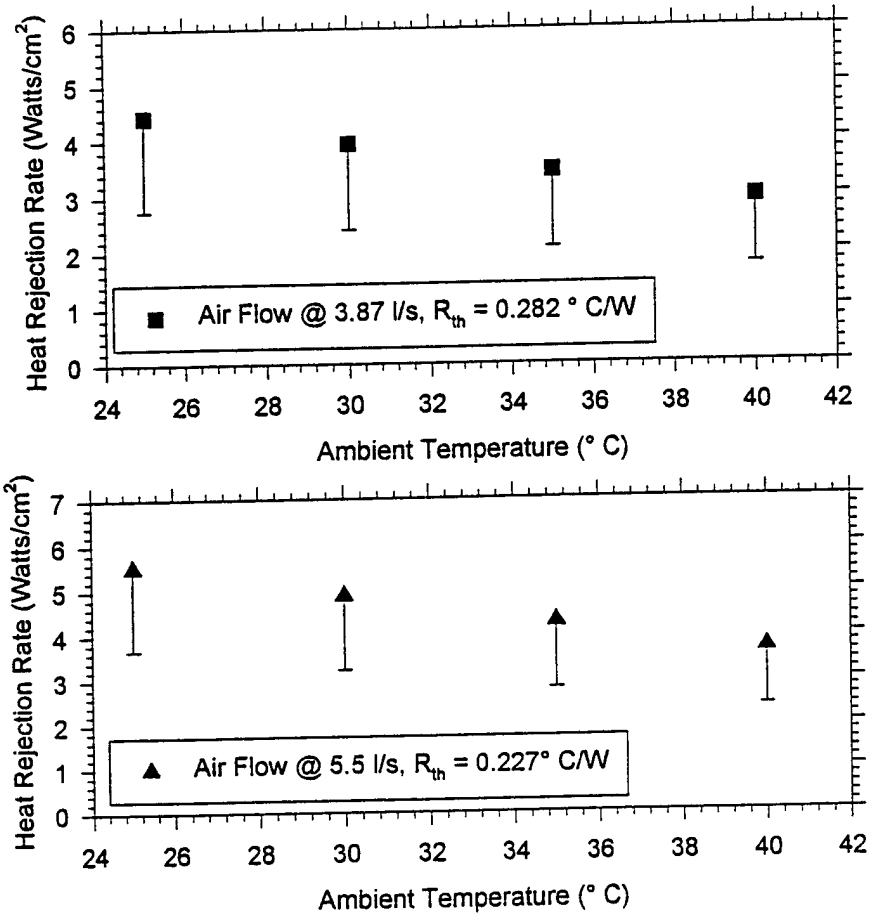

Figure 9. Heat rejection rates of configuration (iii) heat sink (B)-PV in three air flow rates (see text for configuration (iii) and heat sink (B) description).

For heat sink-PV cell assembly (iii), instead of repeating the same calculation, we calculated the air temperature and sink temperature at the exit and limits the heat input rate over the entire PV cell to 108 Watts (3 W/cm^2 x 36 cm^2). The heat sink temperature rise over the air temperature at any location is calculated as [Wakefield Catalog 1996, p.9]:

$$\Delta T_{SINK} = \text{thermal resistance of assembly x input rate} = (\theta_{CS} + \theta_{JC} + \theta_{SA})\ ^\circ C/W \times 108\ W$$

and $$T_{SINK\ AT\ THE\ EXIT} = T_{OUT} + \Delta T_{SINK}$$

The results are tabulated in **Table 11**. In the column 9, only those numbers in bold meet the upper sink temperature limit of 70 °C. Both tables give rise to the similar conclusion. In order to use forced-air cooling, air flow rate should be greater than 5.5 l/s (11.7 cfm) to meet the PV tempetature limit of 70 °C. It should be noted that these values were obtained with 4 Watts of blower power, therefore, at least 10 percent generated power will be used to cool the PV arrays (for a 40% efficient concentrator PV array: power consumption is 4W, then 4W÷(2.75 W/cm^2 x 36 cm^2 x 0.4) = 0.1).

Table 11. Summary of the performance of the configuration (iii) heat sink (B)/PV assembly in several ambient air temperatures and air flow rates under an uniform heat input of 108 Watts. The last column is the heat sink temperature at the heat sink exit.

PV/heat sink assembly (iv)	T_∞ (°C)	Q (W)	Q" (W/cm^2)	$\Delta T'$ ($T_{OUT}-T_{IN}$)	T_{OUT} (°C)	T_{AVE} (°C)	ΔT_{SINK} @ exit (°C)	T_{SINK} @ exit (°C)
Cases (a) Thermal resistance of assembly = 0.388 °C/W								
Air flow 2.5 l/s (5.3 cfm)	25	116	3.2	36	61	43	42	85
	30	103	2.9	37	67	48	42	90
	35	90	2.5	37	72	54	42	96
	40	77	2.1	38	78	59	42	101
Case (b) Thermal resistance of assembly = 0.253 °C/W								
Air flow 3.87 l/s (8.2 cfm)	25	178	4.9	23	48	37	27	*67*
	30	158	4.4	24	54	42	27	*69*
	35	138	3.8	24	59	47	27	74
	40	119	3.3	25	65	52	27	79
Case (c) Thermal resistance of assembly = 0.198 °C/W								
Air flow 5.5 l/s (11.7 cfm)	25	227	6.3	16	41	33	21	*54*
	30	202	5.6	17	47	38	21	*59*
	35	177	4.9	17	52	43	21	*64*
	40	152	4.2	17	57	49	21	70

Italic indicates workable conditions.

d.6. Recuperator Design and Testing

The generator design has some recuperation because the exhaust gas exiting the top reflector opening heats the incoming fuel and air mixture. Outside the generator, the temperature of fuel mixture inside the U-tube reached 208-215 °C at the location just above the mantle emitter. To enhance the recuperation further, a compact recuperator structure was built and soldered onto the U-tube, two inches above the mantle (**Figure 10**). A high temperature alloy screen with a wire diameter of 0.028 inches and 8 mesh opening was rolled into a spiral. The inner portion of the spiral was welded on the fuel U-tube. The outer portion was welded to a low carbon steel tube of 1.5 inches diameter to form a recuperator. This simple recuperator cylinder allowed more heat to be captured by funneling a large portion of the hot exhaust gas through the metal screen. With this recuperation, the temperature inside the U-tube increased to 200-250 °C at the same location (propane gas, 40 psi orifice pressure and 12.5 scfh).

After inserting the combustion burner inside TPV generator and adding both reflectors, the temperature of the fuel mixture went above 420 °C. This temperature is also influenced by the fuel flow rate. Therefore, the top reflector opening had to be enlarged to maintain the

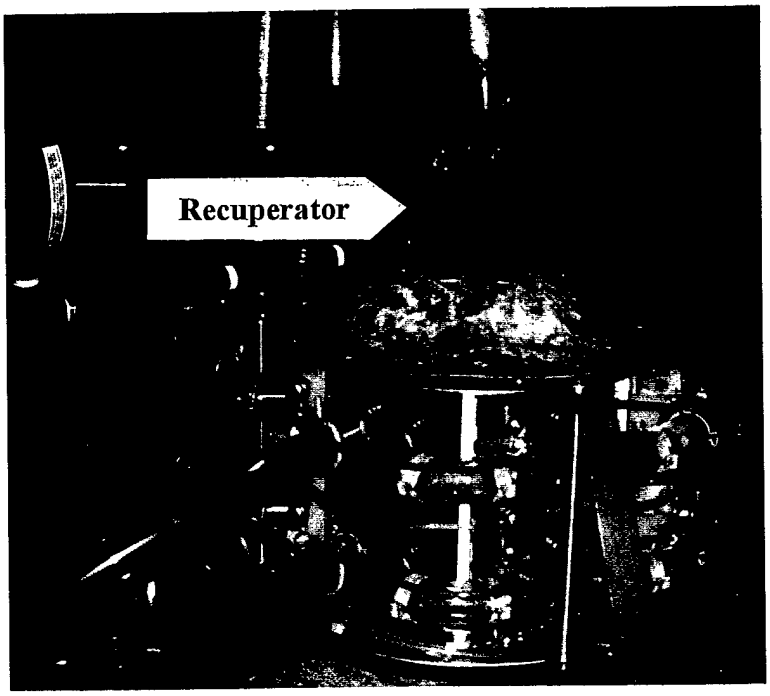

Figure 10. Compact recuperator was being tested for increasing the power output.

temperature below 400 °C. The maximum power output of 112.5 Watts was obtained at orifice pressure of 40 psi., flowmeter pressure at 42 psi. and gas flow rate at 12.5 scfh.(fuel input rate 9566 Watts (32,600 Btu/hr)).

d.7. Electrical Power Output Measurement

Initial tests produced power outputs ranging from 33-90 Watts (**Table 12**). Moving the PV cells as close as to the emitter but outside the plume of the exhaust hot gas, and adjusting the distance between nozzle and fuel input, resulted in 98.5 Watts. The power output reached 90-107 Watts (no load) by adding both reflectors. The average power output from the top six PV arrays was higher than those lower six level cells because of the larger opening in the top reflector. With the addition of recuperator, the generator had a no-load maximum power output of 112.5 Watts. The power output under load was measured on a 6 cm x 6 cm single PV array in the generator (**Figure 11**). The maximum power output is 10.0 Watts. Therefore, the maximum power output of the generator is calculated to be 120 Watts for fuel input rate of 9566 Watts. The fuel to electric conversion are ranging from 1-2%. The fuel to electric conversion value should be higher since some fuel loss occurred at the nozzle and fuel tube inlet, and the optical loss at reflector surface. When considering a self-sustaining TPV generator, at least 50 Watts of power will be needed for cooling the PV array, therefore, a net 50 watts power output will be obtained. This 50 Watts self-sustaining unit can serve as a modular system which can be increased in number for any power output desired within the range of 100 to 500 watts.

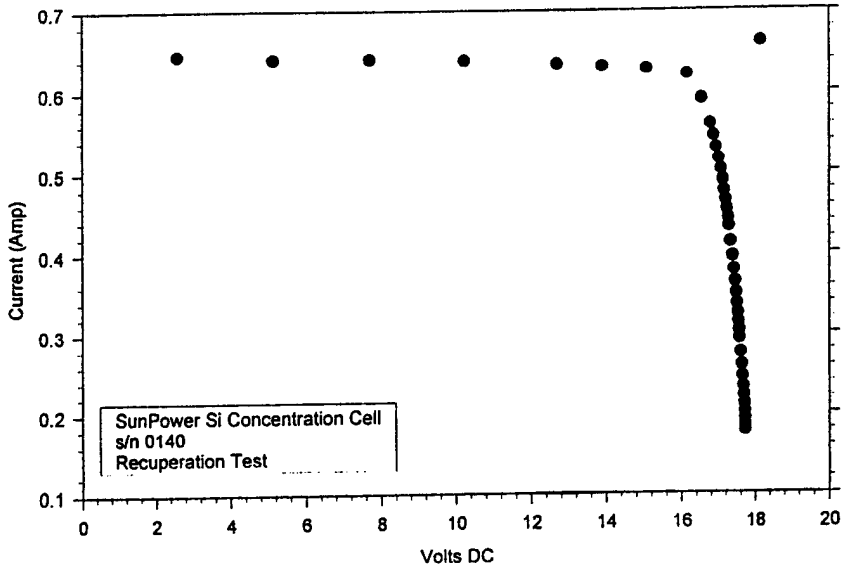

Figure 11. The voltage-current curve measured on a single PV array in the TPV generator under for determining the maximum power output

Table 12. Generator power outputs under different fuel input rates.

Conditions	(C_3H_8) Fuel Flow (un-correct.) scfh	Rota-meter Press. (psig)	(C_3H_8) Fuel Flow (correct.) scfh	Fuel Energy (Watts)	PEP-100 Power (ff=0.81) (Watts)	Fuel-to-electric (%)	Mantle Loading (W/cm^2)
5" mantle, 7°C	3	10	3.15	2,306	32.5	1.41	15.2
water, quartz	4	30	5.66	4,137	56.8	1.37	27.2
bottom reflector	4.5	50	7.66	5,599	76.7	1.37	36.8
only.	4.7	60	8.59	6,283	86.6	1.38	41.3
5" mantle, 7°C	3	10	3.15	2,306	37.2	1.61	15.2
water, quartz	4	30	5.66	4,137	57.9	1.40	27.2
bottom & top	4.7	50	8.00	5,848	80.9	1.38	38.5
steel flat reflector	4.8	60	8.78	6,417	79.7	1.24	42.2
5" mantle,	3	10	3.15	2,306	32.3	1.40	15.2
4° C water,	3.8	30	5.37	3,930	62.3	1.59	25.9
bottom reflector	4.5	50	7.66	5,599	81.1	1.45	36.8
only	4.7	60	8.59	6,283	86.5	1.38	41.3
	4.8	70	9.35	6,833	90.0	1.32	45.0
5.5" mantle,	8	42	12.60	9,566	112.5	1.18	-
7°C water	8	42	12.60	9,566	111.6	1.17	-
bottom reflector	8	42	12.60	9,566	109.9	1.15	-
with recuperator	8	42	12.60	9,566	108.9	1.14	-

E. TPV GENERATOR PORTABILITY ENHANCEMENT

e.1. Generator Shock Isolation and Drop Test

In the early part of the program, an attempt to shock isolate the emitter mantle from the combustion manifold was made by suspending the ytterbia mantle on a ceramic ring attachment, which was fabricated from a castable ceramic materials (RESCOR 740™, Cotronics Corp. Brooklyn New York. This ring was supported by Kanthal metal alloy springs. The design had a considerable lost in efficiency due to hot combustion gases escaping from the annulus between the combustion mixture manifold and the ceramic ring, lowering the emitter temperature. Thereafter, shock isolation was sought to apply to the entire generator.

To shock isolate the entire generator, we selected and mounted shock absorbers to demonstrate its effectiveness in increasing mantle impact tolerance. We designed and built a drop test fixture for a consistent and repeatable drop test. The fixture consisted of three vertical unistrut channels and a dummy generator. The dummy generator was guided by the unistrut and free-fall onto the base (**Figure 12**). The dummy generator had the same dimension and gross weight (10 kilograms) as the real TPV generator and had a mantle attachment allowing burnt mantles to be quickly replaced and tested.

We selected a hydraulic shock absorber (SALD-3/8X1-S, Enertrols, Inc. Westland, Michigan) to provide true linear deceleration during the generator impact. A rotation dial adjusted the shock absorbers to the desirable deceleration rate for a range of specific combination of velocity and propelling force. Three absorbers were used to moderate the impact.

Eight resetable impact indicators (type OMNI-G from Impact-o-graph®, Chatsworth Data Corporation, Chatsworth, California; Switch set points of 10, 15, 25, 50, and 100 g ± 20% or 2 "g") were attached to the sides of the generator to validate the impact force and to tune the shock absorbers. The shock absorbers were fine-adjusted to minimize the impact force, as indicated by the minimal triggering in the force indicators. The shock tests were carried out by dropping the dummy generator with attached burnt mantles onto the floor base from a fixed height, and thereafter at every two inches increments. To avoid the cumulative effect in mantle damage, tests were repeated 3 times at the height of the last breakage using newly-burnt mantles. The shock tests were again performed without shock absorbers on the newly burnt mantles.

Table 13 shows the results of the impact test. The "P" and "F" indicate the mantles either passed or failed in the tests, respectively. The burnt mantles did not survive even from a drop distance of two inches. The mantles always failed at the location at the ring attachment due to tensile failure. The burnt mantles with shock absorbers survived at 12 inches height. Shorter mantle survived at higher impact force.

In conclusion, while this was still less than the desirable height, the result demonstrated the improvement in mantle survivability through proper shock isolation. The portability of the TPV generator can be further improved by increasing the mantle strength.

Figure 12. The dummy generator with the attached burnt mantle for drop test.

Table 13. Results of shock isolation tests.

Height	G	Without Shock Absorbers			With Shock Absorbers		
(inch)		Mantle 5" long	Mantle 5.2" long	Mantle 4.75" long	Mantle 5" long	Mantle 5.2" long	Mantle 4.75" long
2	2.36	**F**	**F**	**F**	P	P	P
4	4.71	***	***	***	P	P	P
6	7.07	***	***	***	P	P	P
8	9.42	***	***	***	P	P	P
10	11.78	***	***	***	P	P	P
12	14.14	***	***	***	**F**	**F**	P
14	16.49	***	***	***	***	***	**F**

Shock model: SALD-3/8X1-S (ADJUSTABLE SHOCK)

P = Passed F = Failed *** = did not test G = calculated G force

Shock indicators used: 10g, 15g, 25g, 50g, 100g (accuracy: ± 20% or ± 2g)

e.2. *Filament-Wound Emitter Structure Development*

The drop test clearly indicates mantle is a weak link in the TPV generator, and a robust emitter structure is needed for a practical soldier portable generator. Before the STTR Phase I was awarded, Quantum Group, Inc. already explored a metal organic precursor process for stronger rare-earth oxide fiber and emitter structures fabrication. Under an IR&D project, continuous fiber spinning process and uniform microstructure in fibers were demonstrated (**Figure 13**). The fiber also showed the same clean spectra as the mantle type structure. An U.S. patent application was filed and was allowed.

Under this program, we scaled up the precursor quantity and developed several fiber winding techniques to fabricate emitter structures. The goal was to fabricate robust self-supporting emitter structures for portability enhancement via stronger emitter fibers made by well-controlled fiber spinning, pyrolysis and sintering processes.

The emitter structures were made by several methods. In the first method, the precursor fiber was first spun and subsequently loosely packed around a Pyrex® glass tube. The low packing-density structure was weak due to few fiber joints in the structure. The second structure was formed by loosely spinning the fiber onto a rotating and transversely-traveling mandrel. The structure had a "cotton-candy-like" fluffy wall, which might provide better impact resistance than the thin-walled mantle structure. However, this structures had a large fiber diameter—same as that of the spinneret opening of 50 μm—made it difficult to be heat treated. **(Figure 14).**

By increasing the drawing speed relative to extrusion speed, the precursor fiber diameter was reduced to ~30 μm. A circumferential winding pattern emitter structure was made at the maximum cross-winding speeds of 15.5 cm/min, which had an easy-fractured cleavage between to the fiber. The structure tightly adhered to the mandrel and were difficult to be removed due to static charge. Increasing the transverse cross-winding speed to 144 cm/min resulted in a helical winding pattern emitter structure. The helical winding emitter have no easily-fractured cleavage and is a more open structure than the circumferential patterned structure. This adhesion problem was solved by changing mandrel material and adding a paper sleeve on the surface of the mandrel.

The precursor emitter structures have 50 percent linear shrinkage. Inconsistent emitter heat treatment results indicate the fiber diameter, heating rates, organic burnout temperature, and atmosphere are critical. Heat treatment study was continued during the last two months of the Phase I program. During the no cost extension period of this contract, proper heat treatment conditions were found. Fibers of smooth surface and emitter structures without cracks were made. Self-standing crack-free emitter filament-wound structures can be now successfully fabricated **(Figure 15).** It is now possible to test emitter structure strength and performance, and re-examine different emitter structure morphology and designs, such as the fluffy structure made before.

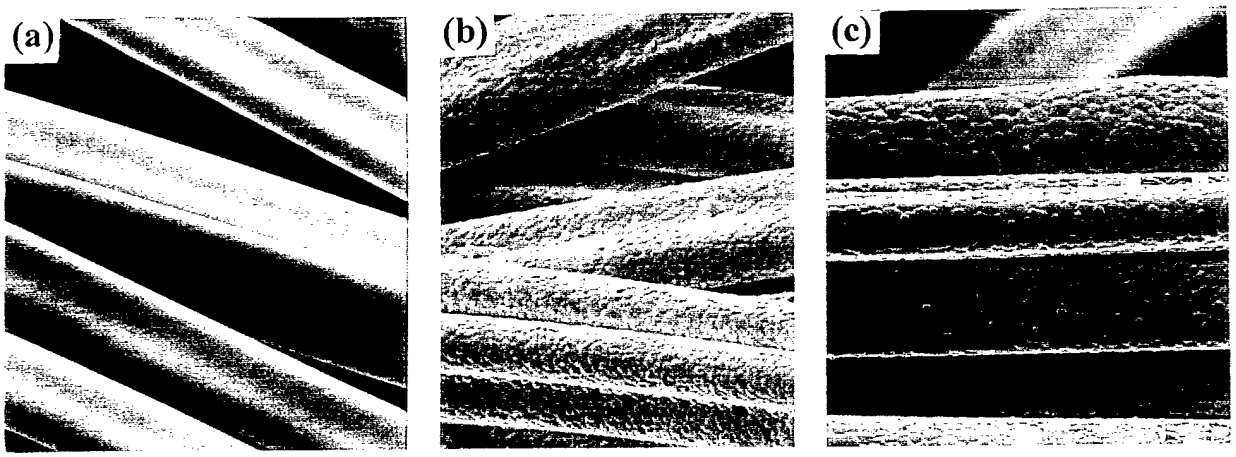

Figure 13. Scanning electron micrographs of metal organic derived Yb_2O_3 emitter fiber after 1 hour heat treatment at (a)1200° C (500x), (b) 1500° C (1000x) and (c) 1600° C (1000x).

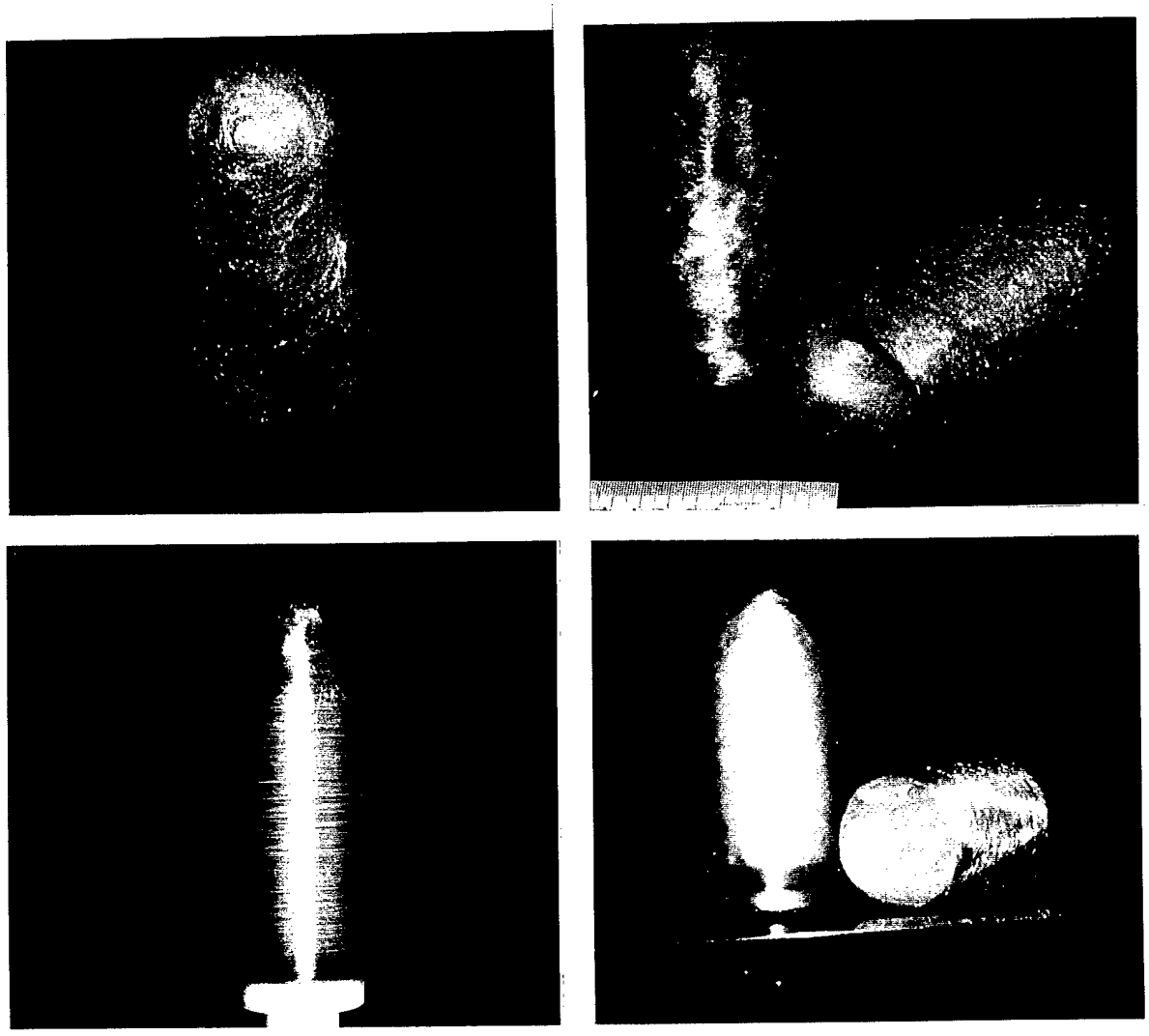

Figure 14. Ytterbia emitter structures made from several filament-winding techniques.

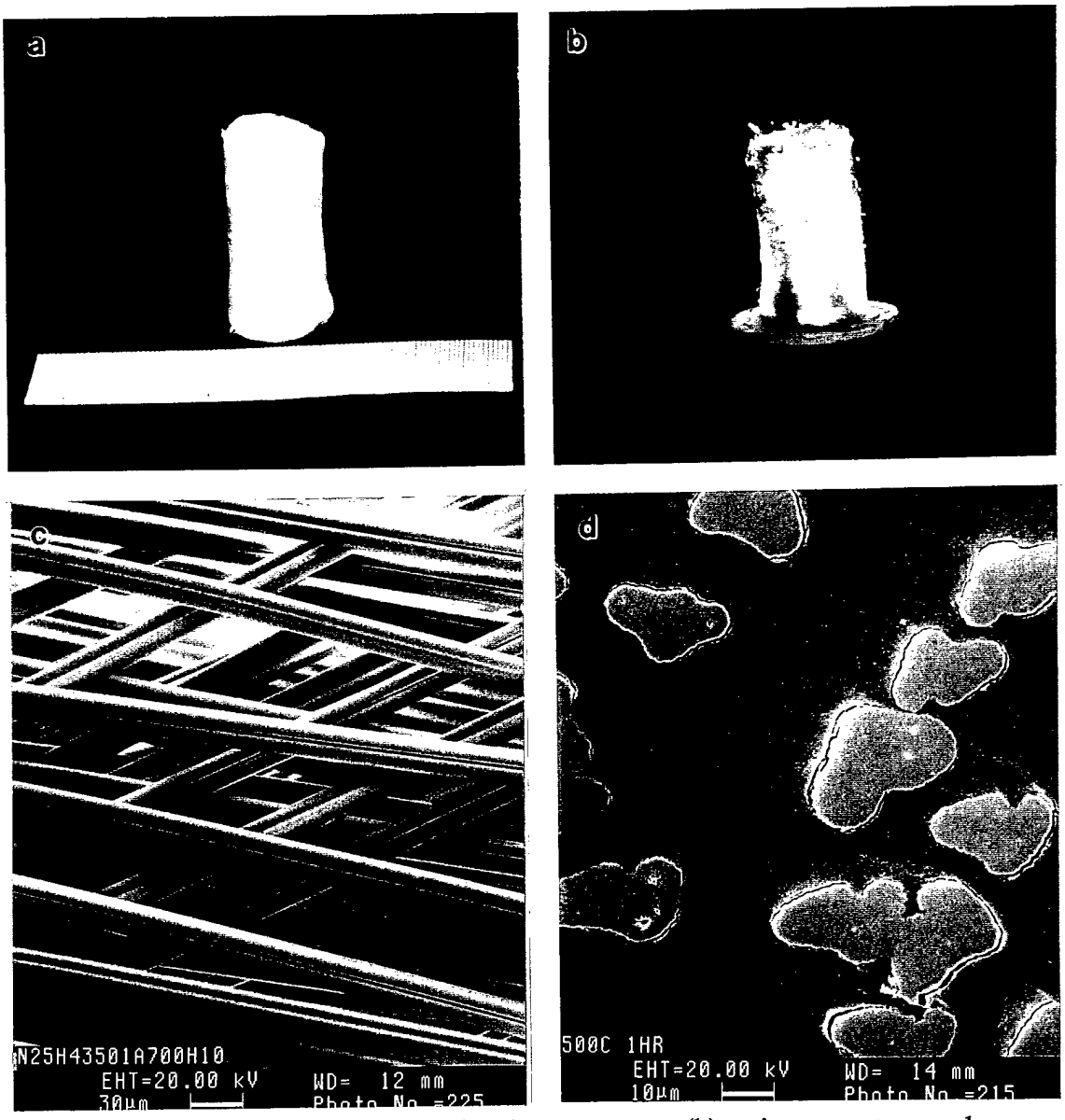

Figure 15. (a) A self-standing helical wound emitter structure, (b) emitter structure under preliminary testing; (c) emitter structure under higher magnification showing opening for easy gas flow; (d) no cracks were observed in polished cross-section of the emitter fiber after heat treatment at 1500 °C.

e.3. Suggested Work for Phase II

The Phase I STTR objective was to examine the potential thermophotovoltaic (TPV) technology to provide 100 Watts of electrical power for the soldier in the field. A laboratory proof-of-concept TPV generator was built, which consists of a propane supply, an atmospheric combustion burner, an ytterbia mantle, a fused silica absorption filter and 12 silicon concentrator arrays cooled by circulating water. This bench-top atmospheric generator demonstrated 112 Watts of electrical

output with fuel to electric conversion of 1-2 %. The potential fuel to photon conversion is estimated to be higher considering various losses (such as some fuel loss, and reflector loss) in the current system. It needs to be fully-integrated and packaged as a single self-sustaining unit before the system efficiency can be determined. Much higher electric power output of 140-180 Watts was obtained by using a pre-mix burner system, but it also created higher heat rejection requirements. The trade-off needs to be examined.

The photovoltaic cell forced-air cooling requirement was evaluated by measuring heat flux and calculating heat transfer of multi-channel heat sinks under different air flow velocities and ambient air temperatures. The maximum heat rejection was 2.8 W/cm^2 for atmospheric combustion design, and 5.5 W/cm^2 for pre-mix combustion design. The result showed that it is feasible to use a forced-air multi-channel heat sink to cool PV cell, provided that the generator has sufficient air flow velocity (> 5.5 l/s or 11.7 cfm) from the blower, operates at no higher than 40 °C ambient air temperature and have low blower power consumption.

The specific challenges to improve the TPV generator for the Phase II program are:

1. Design and fabricate a complete forced air cooling system to simultaneously cool the PV arrays, the absorption filter, and the top reflector with minimal blower power consumption.
2. Improve photon profile and uniformity and match with PV cell arrangement
3. Complete system design, integration, and packaging.
4. Evaluate a multi-fuel use feature.
5. Develop a shock isolation system for other orientation.
6. Increase the mechanical integrity of the emitter;
7. Evaluate optical filters.
8. Reduce the weight of the system;
9. Lower the cost of the generator unit.

A complete assembly of multi-channel heat sink and PV array will be analyzed, built, and tested for the cooling performance under different air velocities and ambient temperatures. Afterward, the system will be integrated and packaged into a complete unit with reflectors, ignition system, cooling blower, and shock absorbers in place for system performance evaluation and system efficiency measurement. The fabrication of robust emitter structures using filament winding approach will be continued. After successful testing, the reduction in the generator weight and cost will be pursued.

F. REPORT OF INVENTIONS

Quantum Group, Inc. intends to disclose or file for U.S. patents for the inventions related to:

1. "Method for Making Rare Earth Oxides Emitter Structures," K.C. Chen
2. "Pre-mix Burner System for Thermophotovoltaic Power Generator," Pedro Samiento.

G. BIBLIOGRAPHY

[ARMY STTR proposal (1995)]."Man Portable TPV Generator System," proposal No. P-35077-RT-ST1.

[ARPA (1996)] "Development of Thermophotovoltaic Generators for (unmanned Underwater Vehicles) Military Application," Final Report for ARPA contract MDA972-93-C-0042, Goldstein, M. K., et. al. (1996).

[CEC (1995)] "TPV Cogeneration for Industrial Water Heating Applications with Low NO_x Emissions," Final Report for California Energy Commission Contract No. 500-90-23, Goldstein, M. K., Kushch, A., Skinner, S. M. (1995).

[Good, B. 1995] Good, B. S., Chubb, D. L., and Lowe, R. A. (1995) "Comparison of Selective Emitter and Filter Thermophotovoltaic Systems," in the Second NREL Conference on Thermophotovoltaic Generation of Electricity, AIP Conference Proceeding 358. Am. Inst. of Phys., New York.

[Kleiner et. al. 1995]. Kleiner, Michael; Kuhn, S. A.; Haberger, K. (1995) "High Performance Forced Air Cooling Scheme Employing Microchannel Heat Exchanger," IEEE Transactions on Components, Packaging, and Manufacturing Technology-Part A, Vol. 18 [4] December 1995.

[Nelson, R 1994] Nelson, R. E., (1994) "Thermophotovoltaic Emitter Development," in the First NREL Conference on Thermophotovoltaic Generation of Electricity, AIP Conference Proceeding 321. Am. Inst. of Phys., New York.

[Wakefield Catalog 1996] Wakefield Engineering 1996 Catalog, Wakefield, Mass. p. 8-9.